Single Spin Asymmetries in charmonium production with ISI and FSI in CGI model

A. V. Karpishkov[1,2], M. A. Nefedov[1], and V. A. Saleev[1,2]

[1] Samara National Research University
[2] Joint Institute for Nuclear Research

28.10.2020
SPD Physics and MC meeting

Outline

1. Generalized Parton Model (GPM) and it's application to calculation of SSA
    - Factorization formula for the GPM
    - Polarized production. SSA
    - Including ISI and FSI – Color Gauge Invariant formulation of GPM
2. SSA in GPM and CGI-GPM
    - Numerical results. Comparison to PHENIX data
    - Numerical results. Predictions for NICA
3. Summary

Generalized Parton Model (GPM) and it's application to calculation of SSA

Factorization schemes in different p_T-regions

The traditional Collinear Parton Model (CPM) is applicable in a region of high-p_T production

$$\mu \sim p_T \gg \Lambda_{QCD},$$

so we can neglect influence of small intrinsic $\mathbf{q_T}$ of initial partons $(\langle q_T^2 \rangle \simeq 1 \text{ GeV}^2)$.

But if we're interested in particle production in a region of $p_T \simeq \sqrt{\langle q_T^2 \rangle} \ll \mu$, we should take into account intrinsic q_T. It can be done within TMD approach, factorization for which has been proven in the limit $q_T \ll \mu$ [J. Collins, Camb. Monogr., Part. Phys. Nucl. Phys. Cosmol. 32, 1-624 (2011)]. In our case, the hard scale μ is given by charmonium mass $m_{\mathcal{C}} = 3.1 \div 3.7$ GeV.
So we can use phenomenological TMD-ansatz, a so called Generalized Parton Model (GPM), initial partons in which are on-shell:

$$q_\mu = xP_\mu^+ + yP_\mu^- + q_{T\mu}, (q_\mu)^2 = 0, \tag{1}$$

and a factorized prescription for TMD parton distribution functions (PDFs) is used:

$$F_a(x, q_T, \mu_F) = f_a(x, \mu_F) G_a(q_T), \tag{2}$$

where $f_a(x, \mu_F)$ – corresponding CPM PDF, $G_a(q_T)$ – Gaussian distribution $G_a(q_T) = \exp(-q_T^2 / \langle q_T^2 \rangle_a) / (\pi \langle q_T^2 \rangle_a)$.

Factorization formula for the GPM

Within the GPM we can write the following expression for the differential cross-section of $2 \to 1$ hard subprocess $g(q_1) + g(q_2) \to \mathcal{C}(k)$:

$$d\sigma(pp \to \mathcal{C}X) = \int dx_1 \int d^2\mathbf{q_{1T}} \int dx_2 \int d^2\mathbf{q_{2T}} \times \\ \times F_g(x_1, q_{1T}, \mu_F) F_g(x_2, q_{2T}, \mu_F) d\hat{\sigma}(gg \to \mathcal{C}), \quad (3)$$

where $\mathcal{C} = J/\psi, \psi(2S)$ or $\chi_c(1P)$, and

$$d\hat{\sigma}(gg \to \mathcal{C}) = (2\pi)^4 \delta^{(4)}(q_1 + q_2 - k) \frac{\overline{|M(gg \to \mathcal{C})|^2}}{2x_1 x_2 s} \frac{d^4k}{(2\pi)^3} \delta_+(k^2 - m_{\mathcal{C}}^2). \quad (4)$$

In a case of $2 \to 2$ subprocess $g(q_1) + g(q_2) \to \mathcal{C}(k) + g(q_3)$, $\mathcal{C} = J/\psi, \psi(2S)$ in formula (3) $d\hat{\sigma}(gg \to \mathcal{C})$ must be replaced by:

$$d\hat{\sigma}(gg \to \mathcal{C}g) = (2\pi)^4 \delta^{(4)}(q_1 + q_2 - k - q_3) \frac{\overline{|M(gg \to \mathcal{C}g)|^2}}{2x_1 x_2 s} \frac{d^3k}{(2\pi)^3 2k_0} \frac{d^4q_3}{(2\pi)^3} \delta_+(q_3^2). \quad (5)$$

Four-momenta of initial partons are on mass-shell ($q_1^2 = q_2^2 = 0$) and have longitudinal (along the Z-axis) and transverse parts:

$$q_1^\mu = \left(x_1 \frac{\sqrt{s}}{2} + \frac{\mathbf{q}_{1T}^2}{2\sqrt{s}x_1}, \mathbf{q}_{1T}, x_1 \frac{\sqrt{s}}{2} - \frac{\mathbf{q}_{1T}^2}{2\sqrt{s}x_1} \right)^\mu, \quad (6)$$

$$q_2^\mu = \left(x_2 \frac{\sqrt{s}}{2} + \frac{\mathbf{q}_{2T}^2}{2\sqrt{s}x_2}, \mathbf{q}_{2T}, -x_2 \frac{\sqrt{s}}{2} + \frac{\mathbf{q}_{2T}^2}{2\sqrt{s}x_2} \right)^\mu. \quad (7)$$

Single Spin Asymmetry

In inclusive process $p^{\uparrow}p \to \mathcal{C}X$ $\mathcal{C} = J/\psi, \chi_c, \psi(2S))$ SSA is defined as:

$$A_N = \frac{d\sigma^{\uparrow} - d\sigma^{\downarrow}}{d\sigma^{\uparrow} + d\sigma^{\downarrow}} = \frac{d\Delta\sigma}{2d\sigma}. \tag{8}$$

The numerator and denominator of A_N have the form:

$$d\sigma \propto \int dx_1 \int d^2q_{1T} \int dx_2 \int d^2q_{2T} F_g(x_1, q_{1T}, \mu_F) F_g(x_2, q_{2T}, \mu_F) d\hat{\sigma}(gg \to \mathcal{C}X), \tag{9}$$

$$d\Delta\sigma \propto \int dx_1 \int d^2q_{1T} \int dx_2 \int d^2q_{2T} [\hat{F}_g^{\uparrow}(x_1, \mathbf{q}_{1T}, \mu_F) - \hat{F}_g^{\downarrow}(x_1, \mathbf{q}_{1T}, \mu_F)] \times F_g(x_2, q_{2T}, \mu_F) d\hat{\sigma}(gg \to \mathcal{C}X), \tag{10}$$

where $\hat{F}_g^{\uparrow,\downarrow}(x, q_T, \mu_F)$ is the distribution of unpolarized gluon (or quark) in polarized proton.
Following the Trento conventions [A. Bacchetta, U. DAlesio, M. Diehl and C. A. Miller, Phys. Rev. D **70**, 117504 (2004)], the gluon Sivers function (GSF) can be introduced as

$$\Delta\hat{F}_g^{\uparrow}(x_1, \mathbf{q}_{1T}, \mu_F) \equiv \hat{F}_g^{(\uparrow)}(x_1, \mathbf{q}_{1T}, \mu_F) - \hat{F}_g^{(\downarrow)}(x_1, \mathbf{q}_{1T}, \mu_F) = \\ = \Delta^N F_g^{\uparrow}(x_1, \mathbf{q}_{1T}^2, \mu_F)\cos(\phi_1) \equiv \left(-2\frac{q_{1T}}{M_p}\right) F_{1T}^{\perp g}(x_1, \mathbf{q}_{1T}^2, \mu_F)\cos(\phi_1). \tag{11}$$

Moreover, GSF must satisfy the positivity bound $\forall\ x_1, q_{1T}$:

$$\left|\Delta^N F_g^{\uparrow}(x_1, \mathbf{q}_{1T}^2, \mu_F)\right| \le 2F_g(x_1, q_{1T}, \mu_F). \tag{12}$$

Single Spin Asymmetry in the CGI-GPM framework

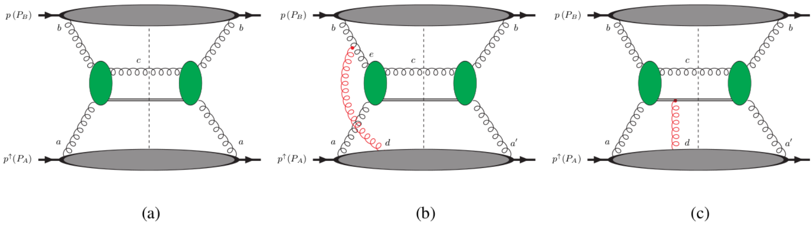

Figure 1 : LO diagrams for the process $p^{\uparrow}p \to J/\psi X$, assuming a color-singlet production mechanism, within the GPM (a) and the CGI-GPM (b), (c). It turns out that only initial state interactions depicted in (b) contribute to the SSA. Figure is from [D'Alesio *et.al.*, Phys. Rev. D **96**, 036011 (2017)].

In GPM (Fig. 1 (a)) we can write the numerator of the asymmetry as follows:

$$d\Delta\sigma \propto \left(-2\frac{q_{1T}}{M_p}\right) F_{1T}^{\perp g}(x_1, \mathbf{q}_{1T}^2, \mu_F)\cos(\phi_1) \otimes F_g(x_2, q_{2T}, \mu_F) \otimes H^U_{gg\to cd}, \quad (13)$$

where $H^U_{gg\to cd} = \overline{|M(gg\to cd)|^2}$.

Single Spin Asymmetry in the CGI-GPM framework

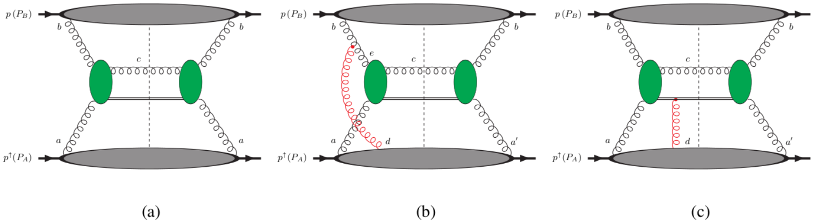

Figure 2 : LO diagrams for the process $p^{\uparrow}p \to J/\psi X$, assuming a color-singlet production mechanism, within the GPM (a) and the CGI-GPM (b), (c). It turns out that only initial state interactions depicted in (b) contribute to the SSA. Figure is from [D'Alesio *et.al.*, Phys. Rev. D **96**, 036011 (2017)].

Formally, the numerator of the asymmetry in the CGI-GPM approach ([L. Gamberg and Z. B. Kang, Phys. Lett. B **696**, 109 (2011)]) can be obtained from eq. (13) by with the substitution:

$$F_{1T}^{\perp g} H^U_{gg\to J/\psi g} \to \frac{C_I^{(f)} + C_{F_c}^{(f)}}{C_U} F_{1T}^{\perp g(f)} H^U_{gg\to J/\psi g} + \frac{C_I^{(d)} + C_{F_c}^{(d)}}{C_U} F_{1T}^{\perp g(d)} H^U_{gg\to J/\psi g} \equiv$$
$$\equiv F_{1T}^{\perp g(f)} H^{Inc(f)}_{gg\to J/\psi g} + F_{1T}^{\perp g(d)} H^{Inc(d)}_{gg\to J/\psi g}. \quad (14)$$

Color factors and Feynman rules in the CGI-GPM framework

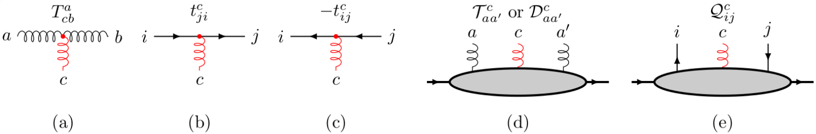

Figure 3 : CGI-GPM color rules for the eikonal three-gluon (a), quark-gluon (b) and antiquark-gluon (c) vertices. The color projectors for the gluon (d) and the quark Sivers functions (e) are shown as well. The eikonal gluon has color index c. Figure is from [D'Alesio *et.al.*, Phys. Rev. D **96**, 036011 (2017)].

The color factors are:

$$\mathcal{T}^c_{aa'} = \mathcal{N}_{\mathcal{T}} T^c_{aa'}, \mathcal{D}^c_{aa'} = \mathcal{N}_{\mathcal{D}} D^c_{aa'}, \mathcal{Q}^c_{ij} = \mathcal{N}_{\mathcal{Q}} t^c_{ij}, \tag{15}$$

where $T^a_{cb} \equiv -if_{acb}$, $D^a_{bc} \equiv d_{abc}$, $\mathcal{N}_{\mathcal{T}} = \frac{1}{Tr[T^cT^c]} = 1/(N_c(N_c^2-1))$,
$\mathcal{N}_{\mathcal{D}} = \frac{1}{Tr[D^cD^c]} = 1/((N_c^2-4)(N_c^2-1))$, $\mathcal{N}_{\mathcal{Q}} = \frac{1}{Tr[t^ct^c]} = 2/(N_c^2-1)$.
So, correspondingly, for the f- and d-type GSF, the relative color factor is therefore calculated from Fig. 1(b) as follows:

$$\boxed{C_I^{(f)} = -\frac{1}{2}C_U, C_I^{(d)} = 0.} \tag{16}$$

And in CSM of the heavy quark-antiquark pair to the FSI, depicted in Fig. 1(c):

$$\boxed{C_{F_c}^{(f)} = C_{F_c}^{(d)} = 0.} \tag{17}$$

SSA in charmonium production at RHIC and NICA

PHENIX-2018 data, $1.2 \leq |y| \leq 2.2$, $\sqrt{S} = 200$ GeV.

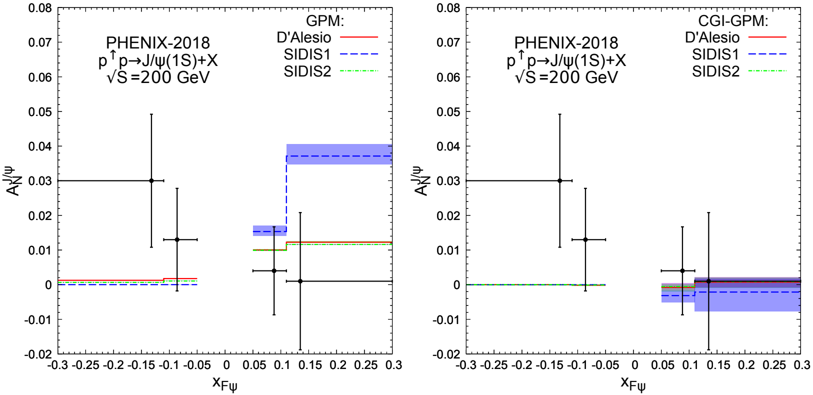

Figure 4 : SSA $A_N^{J/\psi}$ as function of x_F at $\sqrt{s} = 200$ GeV. The theoretical results are obtained in NRQCD with D'Alesio *et al.*, SIDIS1 and SIDIS2 parameterizations of GSFs. Left panel: GPM-prediction. Right panel: CGI-GPM-prediction. Experimental data are from Ref. [C. Aidala *et al.* [PHENIX], Phys. Rev. D **98**, 012006 (2018)].

PHENIX-2018 data, $-2.2 \leq y \leq -1.2$, $\sqrt{S} = 200$ GeV.

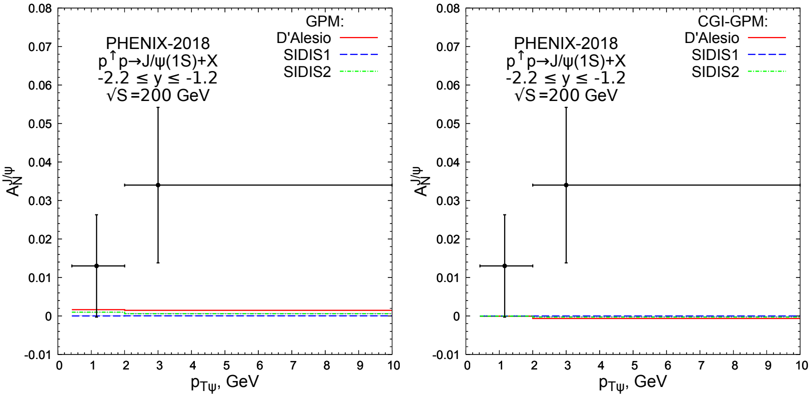

Figure 5 : NRQCD predictions for SSA $A_N^{J/\psi}$ as function of J/ψ-transverse momentum at $\sqrt{s} = 200$ GeV. The theoretical results are obtained with D'Alesio *et al.*, SIDIS1 and SIDIS2 parameterizations of GSFs. Left panel: GPM-prediction. Right panel: CGI-GPM-prediction. Experimental data are from Ref. [C. Aidala *et al.* [PHENIX], Phys. Rev. D **98**, 012006 (2018)].

PHENIX-2018 data, $1.2 \le y \le 2.2$, $\sqrt{S} = 200$ GeV.

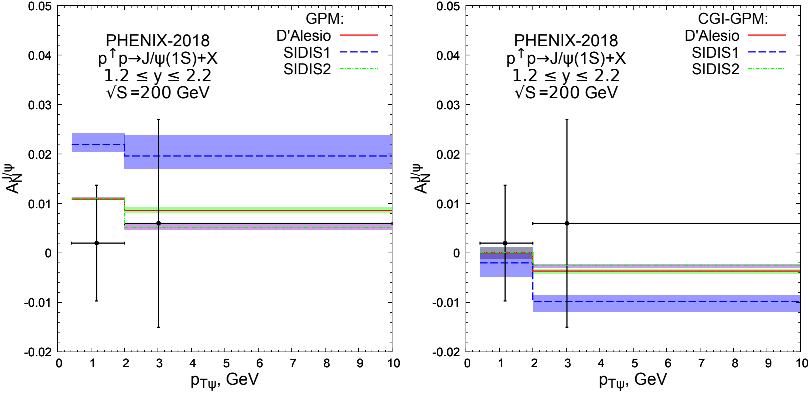

Figure 6 : NRQCD predictions for SSA $A_N^{J/\psi}$ as function of J/ψ-transverse momentum at $\sqrt{s} = 200$ GeV. The theoretical results are obtained with SIDIS1 and D'Alesio et al. parameterizations of GSFs. Left panel: GPM-prediction. Right panel: CGI-GPM-prediction. Experimental data are from Ref. [C. Aidala *et al.* [PHENIX], Phys. Rev. D **98**, 012006 (2018)].

Predictions for SSA at NICA (D'Alesio), $|y| \leq 3$, $\sqrt{S} = 24$ GeV.

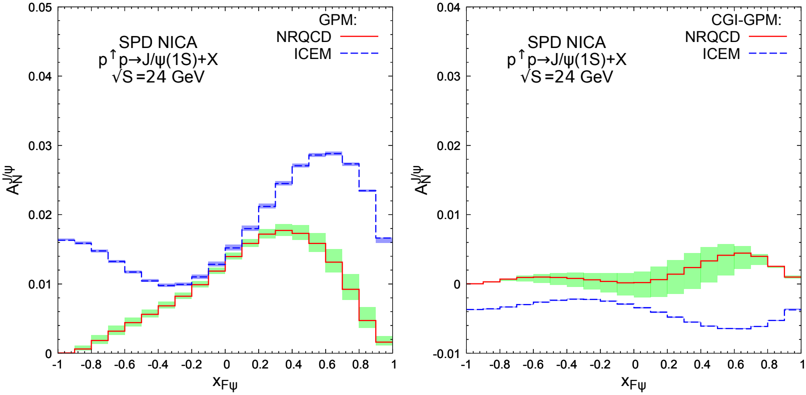

Figure 7 : Comparison of predictions for SSA $A_N^{J/\psi}$ as function of x_F at $\sqrt{s} = 24$ GeV in NRQCD (solid histogram) and ICEM (dashed histogram) approaches. Left panel: GPM-prediction. Right panel: CGI-GPM-prediction. The D'Alesio *et al.* parametrisation of GSFs is used.

Predictions for SSA at NICA (D'Alesio), $|y| \leq 3$, $\sqrt{S} = 24$ GeV.

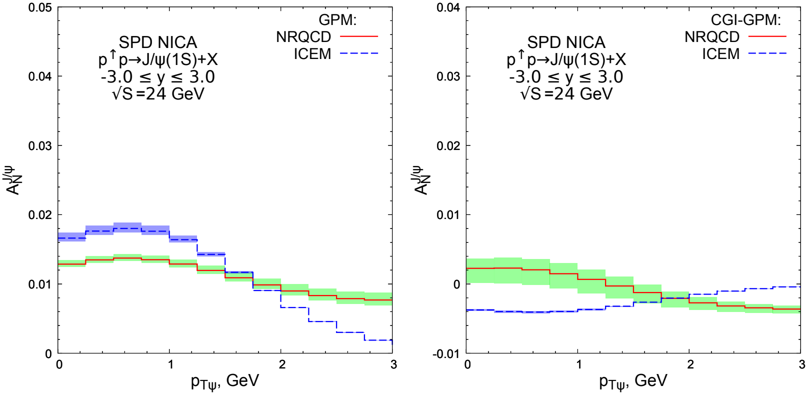

Figure 8 : Comparison of predictions for SSA $A_N^{J/\psi}$ as function of p_T at $\sqrt{s} = 24$ GeV in NRQCD (solid histogram) and ICEM (dashed histogram) approaches. Left panel: GPM-prediction. Right panel: CGI-GPM-prediction. The D'Alesio *et al.* parametrisation of GSFs is used.

Predictions for SSA at NICA (SIDIS1), $|y| \leq 3$, $\sqrt{S} = 24$ GeV.

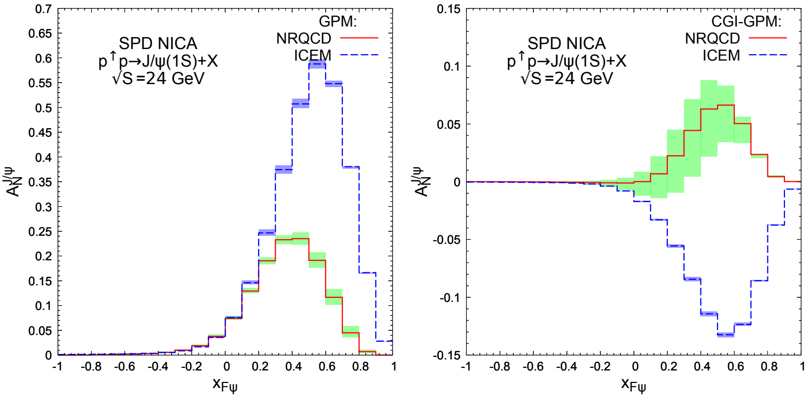

Figure 9 : Comparison of predictions for SSA $A_N^{J/\psi}$ as function of x_F at $\sqrt{s} = 24$ GeV in NRQCD (solid histogram) and ICEM (dashed histogram) approaches. Left panel: GPM-prediction. Right panel: CGI-GPM-prediction. The SIDIS1 parametrisation of GSFs is used.

Predictions for SSA at NICA (SIDIS1), $|y| \leq 3$, $\sqrt{S} = 24$ GeV.

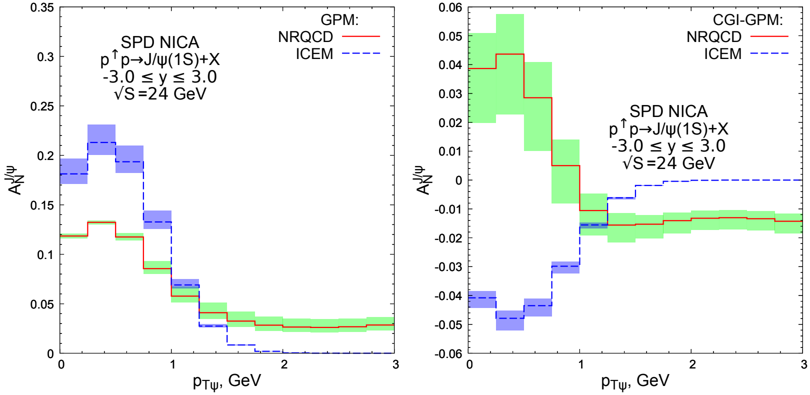

Figure 10 : Comparison of predictions for SSA $A_N^{J/\psi}$ as function of p_T at $\sqrt{s} = 24$ GeV in NRQCD (solid histogram) and ICEM (dashed histogram) approaches. Left panel: GPM-prediction. Right panel: CGI-GPM-prediction. The SIDIS1 parametrisation of GSFs is used.

Predictions for SSA at NICA (SIDIS2), $|y| \leq 3$, $\sqrt{S} = 24$ GeV.

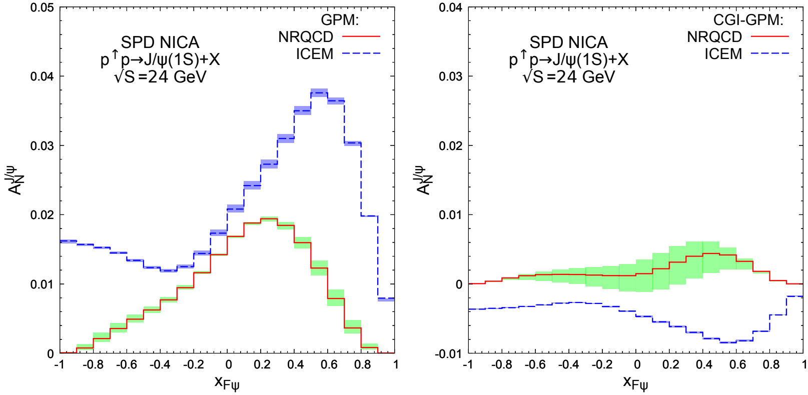

Figure 11 : Comparison of predictions for SSA $A_N^{J/\psi}$ as function of x_F at $\sqrt{s} = 24$ GeV in NRQCD (solid histogram) and ICEM (dashed histogram) approaches. Left panel: GPM-prediction. Right panel: CGI-GPM-prediction. The SIDIS2 parametrisation of GSFs is used.

Predictions for SSA at NICA: NRQCD vs. ICEM (D'Alesio), $|y| \leq 3$, $\sqrt{S} = 24$ GeV.

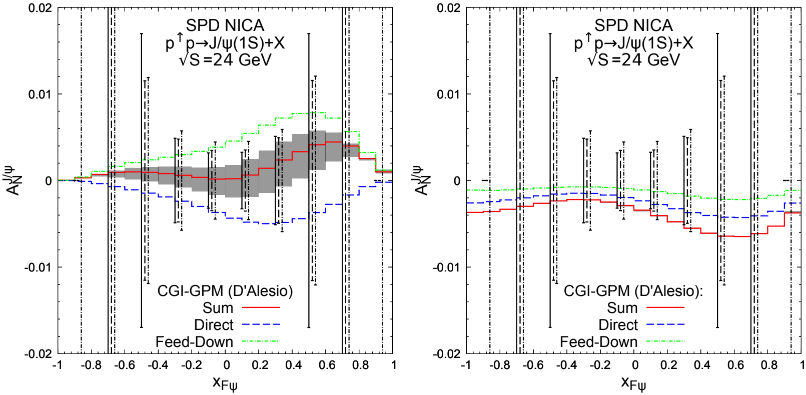

Figure 12 : Comparison of predictions for SSA $A_N^{J/\psi}$ as function of x_F at $\sqrt{s} = 24$ GeV in NRQCD (left panel) and ICEM (right panel) approaches. The D'Alesio *et al.* parametrisation of GSFs is used. Estimation of errors for $A_N^{J/\psi}$ are provided by [I. Denisenko].

Predictions for SSA at NICA: NRQCD vs. ICEM (SIDIS1), $|y| \leq 3$, $\sqrt{S} = 24$ GeV.

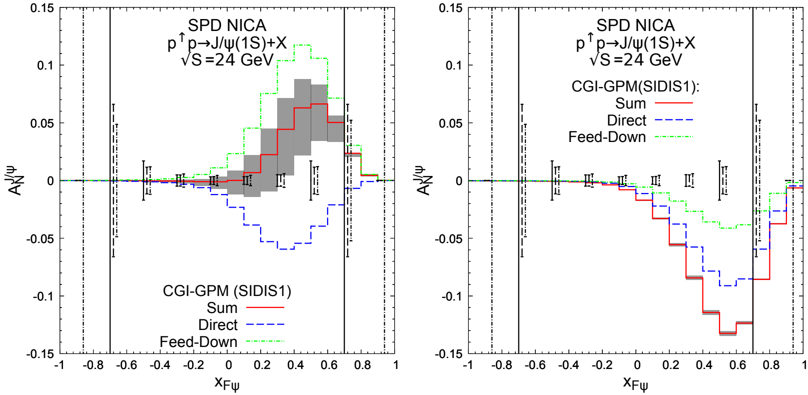

Figure 13 : Comparison of predictions for SSA $A_N^{J/\psi}$ as function of x_F at $\sqrt{s} = 24$ GeV in NRQCD (left panel) and ICEM (right panel) approaches. The SIDIS1 parametrisation of GSFs is used. Estimation of errors for $A_N^{J/\psi}$ are provided by [I. Denisenko].

Predictions for SSA at NICA: NRQCD vs. ICEM (SIDIS2), $|y| \leq 3$, $\sqrt{S} = 24$ GeV.

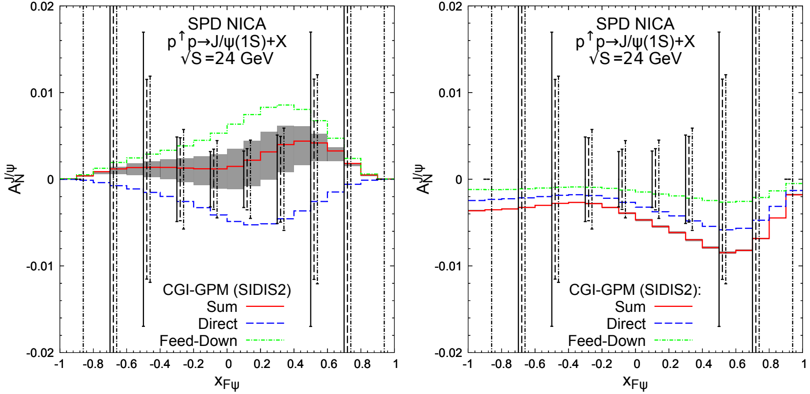

Figure 14 : Comparison of predictions for SSA $A_N^{J/\psi}$ as function of x_F at $\sqrt{s} = 24$ GeV in NRQCD (left panel) and ICEM (right panel) approaches. The SIDIS1 parametrisation of GSFs is used. Estimation of errors for $A_N^{J/\psi}$ are provided by [I. Denisenko].

Summary

- The CGI-GPM formalism, which includes effects of ISIs and FSIs under a one-gluon exchange approximation, can reproduce the twist-3 collinear factorization formalism (see [L. Gamberg and Z. B. Kang, Phys. Lett. B **696**, 109 (2011)] and [D'Alesio *et.al.*, Phys. Rev. D **96**, 036011 (2017)] for details).
- The Color Gauge Invariant formulation of the GPM is able to reproduce the expected opposite relative sign of the Sivers asymmetries, due to the effects of FSIs and ISIs.
- In CGI-GPM within both the frameworks of CSM and ICEM the process $p^{\uparrow}p \to \mathcal{H}X$ of *direct production* of $J/\psi(\psi')$ is sensitive to f-type GSF. While the χ_c production within the CSM is sensitive to d-type GSF and to f-type within the ICEM.
- In the CSM it is better to measure separately direct and feed-down contributions to the J/ψ asymmetry (at least for D'Alesio and SIDIS2 parametrizations). While in the ICEM it is better to look at the *sum* of both contributions.

Thank you for your attention!